Vortex-antivortex coexistence in Nb-based superconductor/ferromagnet heterostructures

F. Bobba,[1,2,*] C. Di Giorgio,[1] A. Scarfato,[1,2,3] M. Longobardi,[3] M. Iavarone,[4] S. A. Moore,[4] G. Karapetrov,[5] V. Novosad,[6] V. Yefremenko,[6] and A. M. Cucolo[1,2]

[1] *"E.R. Caianiello" Physics Department and NANOMATES, Research Centre for Nanomaterials and Nanotechnology, University of Salerno, Fisciano (SA), Italy*

[2] *CNR-SPIN Salerno, Fisciano (SA), Italy*

[3] *University of Geneva, Department of Condensed Matter Physics, CH-1211 Geneva 4, Switzerland*

[4] *Physics Department, Temple University, Philadelphia, Pennsylvania 19122, USA*

[5] *Physics Department, Drexel University, Philadelphia, Pennsylvania 19104, USA*

[6] *Materials Science Division, Argonne National Laboratory, Argonne, Illinois 60439, USA*

(Received 12 March 2014; revised manuscript received 2 May 2014; published 4 June 2014)

Low-temperature magnetic force microscopy was used to study the threshold of nucleation of spontaneous vortex-antivortex structures in superconductor/ferromagnet (S/F) hybrid systems. We investigated S/F heterostructures composed of Py as the magnetic material and Nb as the superconductor, with different thicknesses of Py and Nb. The condition for nucleation of spontaneous vortex-antivortex structures depends on fundamental parameters such as the superconducting penetration depth and the coherence length, as well as on the thickness of the superconducting film and the magnetic domain width. We compare our experimental results with those of existing theoretical models and provide an estimate of the threshold of the local out-of-plane component of the magnetization for different Py film thicknesses.

DOI: 10.1103/PhysRevB.89.214502 PACS number(s): 74.25.Uv, 74.78.Fk, 74.25.Ha

I. INTRODUCTION

Many recent superconducting applications have been enabled by the advances in the understanding of the vortex matter. In fact, the superconducting critical current depends on the static and dynamic behavior of the quantized flux lines, or vortices, which appear in type-II superconductors in the presence of an external magnetic field. In the past, an enhancement of the critical current was obtained by introducing ad hoc defects into superconductors to locally suppress superconductivity and to impose a pinning potential for vortices. Several works have reported enhancement of critical current as a consequence of micrometer size holes, magnetic nanoparticles, and ferromagnetic dots [1–6]. However, in these types of pinning structures, an external magnetic field has to be applied to nucleate vortices and the pinning potential may not be strong enough to prevent the depinning effects caused by the Lorentz force and the thermal fluctuations.

The goal of our work is the direct observation of "spontaneous" vortices that appear in the absence of an external magnetic field in superconductor/ferromagnet (S/F) heterostructures [7–9] created with Nb/Py (permalloy, $Ni_{80}Fe_{20}$) thin films. Techniques which can provide direct observation of vortices in real space at the nanoscale are mainly based on scanning probe microscopies (SPM). Among them, the magnetic force microscopy (MFM) technique has the advantage over scanning tunneling microscopy of being sensitive to vortex polarity and to the underlying magnetic template [10,11]. Recently, the MFM technique was used by the authors to visualize the vortex chains in Nb/Py bilayers as well as their guided motion due to magnetic pinning [12–14], but, to date, measurements of spontaneous vortices in planar S/F hybrids have been performed only on Nb (200 nm)/Py (4 μm) bilayers [12].

In this work, we used low-temperature MFM to investigate the conditions of spontaneous vortex formation in Nb/Py bilayers with different thicknesses of Nb and Py layers. In our samples, the Nb and the Py films are separated by a thin SiO_2 insulating layer to prohibit proximity effects.

In Nb/Py heterostructures, the Curie temperature T_C of Py is much greater than the superconducting critical temperature T_S, ensuring a field cooling of the Nb film in a spatially nonuniform magnetic field. In Py films, stripe magnetic domains are a consequence of canted magnetization vectors, mainly oriented along the film plane but with small alternating up-and-down out-of-plane components [13]. The periodic out-of-plane stray field coming out from the film surface plays the role of a magnetic confinement potential for vortices in the Nb layer [11,16]. In addition, this magnetic template enables vortices to be guided along the magnetic domain, allowing new key experiments in vortex dynamics to be implemented and new devices to be developed.

Here, our experimental MFM results are presented as a quantitative comparison with recently proposed theoretical models [17–19]. In particular, Laiho *et al.* [18] describe the physics of vortices in S/F bilayers in which the ferromagnet exhibits alternating up-and-down out-of-plane magnetization vectors $\pm M_0$. In this picture, the threshold magnetization values required to nucleate spontaneous straight vortices which start and end at opposite faces of the superconducting film and semiloop vortices which start and end within the superconducting film itself were deduced for given values of the stripe domain width w of the F layer, the superconducting penetration depth λ, and the thickness d_s of the S film. In agreement with the model, in the Nb/Py system, the vortex formation is due to the $\pm M_0$ out-of-plane components of Py magnetization. Hereinafter, we define vortices (V) or

*fbobba@unisa.it.

antivortices (AV) as quantum fluxes formed on the top of the $-M_0$ or $+M_0$ domain, respectively.

Within the constraints of the considered model [18], $\frac{w}{\lambda} > 1$ and $\frac{d_s}{\lambda} > 1$, by minimizing the total free energy of the S/F system, the critical magnetization needed to nucleate the first straight V-AV pair or to form the first semiloop results, respectively, in $M_{cs} = 0.2\frac{d_s}{w}H_{c1}$ or $M_{cl} = \frac{H_{c1}}{8\ln(4w/\pi\lambda)}$. Spontaneous vortex formation will thus be energetically regulated by the threshold condition:

$$M_0 > M_{c(s,l)}.$$

Obviously, if $M_{cl} > M_{cs}$ the formation of straight vortices is energetically favored, and vice versa. Moreover, we note that when the F layer thickness is kept fixed, the spontaneous formation of straight vortices in an S film will ensure spontaneous vortex nucleation whenever the S layer is thinner.

In order to quantitatively compare our results with those of the theoretical models, the experimental variables of the threshold condition were characterized. Nb and Py thicknesses were controlled by the thin film deposition protocol, as well as by x-ray diffraction measurements. The magnetic domain width w was extracted directly from MFM maps, and $H_{c1}(T)$ was obtained from $\lambda(T)$ and $\xi(T)$ derived from transport and magnetic measurements. On the other hand, a correct estimate of the out-of-plane component M_0 is not straightforward. In principle, it can be obtained using MOKE (magneto-optical Kerr effect) [20–23], VSM (vibrating sample magnetometry) [24], GME (generalized magneto-optical ellipsometry) [25,26], or by other experimental techniques based on torque magnetometry [27–29]. However, such techniques need to apply an external magnetic field that can considerably change the orientation of the magnetization, leading to a large uncertainty. Moreover, these values would be averaged over the sample surface and could be quite distant from the local values.

In the present work, the MFM imaging of spontaneous V-AV in Nb/Py bilayers, for different Nb and Py thicknesses, is also proposed as an indirect but quantitative method to estimate the M_0 value of our samples.

II. MATERIALS AND METHODS

We fabricated Nb/SiO_2/Py heterostructures with 1-, 2-, and 4-μm Py layers and Nb thicknesses in the range 50–360 nm. In order to magnetically couple but electronically decouple the F and S layers, a 10 nm thin insulating SiO_2 layer was placed between them. Py films were deposited by dc sputtering from a $Ni_{80}Fe_{20}$ target onto a Si substrate at a base pressure of 1.5×10^{-7} Torr, followed by a 10-nm SiO_2 layer. The Nb films were deposited by dc sputtering at room temperature in a dedicated system with a base pressure of 2×10^{-8} Torr.

The behavior of the Nb/Py heterostructures was analyzed by means of a cryogenic UHV scanning force microscope equipped with a magnetic tip and operating in frequency modulation–magnetic force microscopy (FM-MFM) mode. The frequency shift $df = f - f_0$ of the resonating cantilever was acquired, where f is the oscillation frequency measured during tip-sample interaction and f_0 is the free frequency. MFM maps were obtained by scanning at constant tip-sample heights in the range 30–200 nm and the attractive/repulsive tip-sample interaction is mapped using color contrast. During the scanning time, the temperature stability was within 0.01 K. The MFM maps shown below have scan areas of 3.8 μm × 3.8 μm or 2.9 μm × 2.9 μm. For each sample, we scanned several different areas of the surface so as to ensure that significant statistics were obtained. To facilitate the comparison of MFM maps above and below the superconducting critical temperature, the same tip-sample separation was used and the image contrast was rescaled to the same frequency range. In order to get quantitative information from MFM experiments, we need to characterize the three interacting systems, i.e., the magnetic tip, the superconducting Nb layer, and the ferromagnetic Py layer.

We used a commercial Si cantilever, covered with ferromagnetic Co/Cr film, with resonance frequency $f_0 \approx 75$ kHz, elastic constant $k \approx 2.8\ N/m$, and nominal low magnetic moment $\mu \approx 0.3 \times 10^{-13}$ emu. The tip coercivity $H_{\text{tip}}^{c} \approx 550 \div 600$ G was deduced from the inversion of the magnetic contrast by applying an external magnetic field. This relatively high coercivity value excludes the possibility of tip magnetization inversion during the MFM experiments. Before measuring, the tips were magnetized in a downward direction along their longitudinal axis. As a consequence, an attractive (repulsive) force appears as a dark (bright) contrast region in the MFM maps. In presence of vortices, V (AV) appear as darker (brighter) spots on the magnetic background. We remark that the tip-sample distance plays a key role during the MFM experiments. When crossing T_S, the cantilever was pulled away from the sample surface (about 10 μm), to minimize the influence of the tip's stray field on V-AV formation and configuration. Below T_S, we verified that the optimal scanning height was in the range 60–200 nm. Indeed, at smaller tip-sample separation ($d_{ts} < 60$ nm) the stray field of the magnetic tip can induce vortex formation and/or movements, whereas for higher separation values ($d_{ts} > 200$ nm) MFM sensitivity was significantly reduced.

The Nb films were characterized by both transport and magnetic measurements, showing a superconducting critical temperature of $T_S = 8.9 \pm 0.1$ K. From transport measurements [12] and by using the dirty limit expression as derived by Gor'kov [30], $\xi(0\,\text{K}) \approx 12$ nm and $\lambda(0\,\text{K}) = 1.63k\xi(0\,\text{K}) \approx 61$ nm were inferred, where k is the Ginzsburg-Landau parameter. As a consequence, the superconducting lower critical field was calculated to be

$$H_{c1}(0\,\text{K}) = \frac{\Phi_0}{4\pi\lambda(0\,\text{K})^2}\ln\left(\frac{\lambda(0\,\text{K})}{\xi(0\,\text{K})}\right) = 720\,\text{G}.$$

At the measurement temperature of 6 K we have

$$\lambda(6\,\text{K}) = \frac{\lambda(0\,\text{K})}{\sqrt{1-\left(\frac{T}{T_S}\right)^2}} \approx 68\ \text{nm},$$

$$\xi(6\,\text{K}) = \xi(0\,\text{K})\sqrt{\frac{T_S}{T-T_S}} \approx 21\ \text{nm},$$

$$H_{c1}(6\,\text{K}) = \frac{\Phi_0}{4\pi\lambda(6\,\text{K})^2}\ln\left(\frac{\lambda(6\,\text{K})}{\xi(6\,\text{K})}\right) = 418\ \text{G}.$$

Py is a ferromagnetic material where competing magnetic energies (magnetostatic, exchange, magnetoelastic, domain

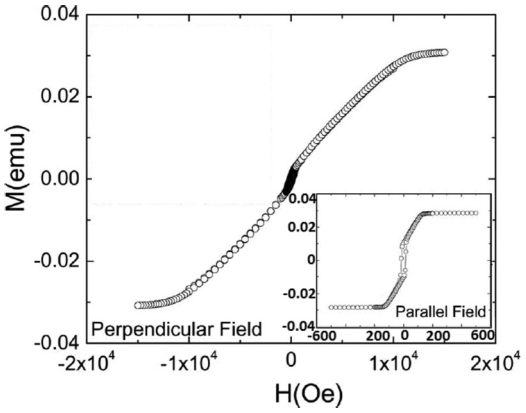

FIG. 1. Magnetization loops of 1-μm-thick Py film at $T = 10$ K for the magnetic field applied perpendicular to the film plane (in main panel) and for the magnetic field applied parallel to the film plane (see the inset) [14].

wall, and anisotropy) determine the domain configurations. In thin films, a periodic stripelike configuration occurs above a critical thickness of $t_c = 2\pi(A/K_u)$ [36], where A is the exchange constant and K_u is the perpendicular anisotropy constant [31,32]. In this case, stripe domains appear as a consequence of a slight magnetization canting with respect to the total in-plane orientation. The small out-of-plane components ($\pm M_0$) point alternatively in upward and downward directions across adjacent stripes.

Figure 1 shows the magnetization loops of the 1-μm-thick Py film for both the perpendicular and the parallel field configurations [14]. We directly measure $H_{\perp}^{\rm sat} = 11\,400$ G and $H_{\parallel}^{\rm sat} = 136$ G, confirming the easy axis in the film plane, and we estimate $M_s = \frac{H_{\perp}^{\rm sat}+H_{\parallel}^{\rm sat}}{4\pi} = 900$ G and $K_u = \frac{M_s H_{\parallel}^{\rm sat}}{2} = 63\,000$ erg/cm^3. The 2- and 4-μm-thick Py samples show similar values.

We remark that K_u and consequently the critical thickness t_c can be strongly affected by the deposition parameters [13]. In our case, by considering the typical value $A = 1 \times 10^{-6}$ erg/cm, $t_c = 100$–300 nm is calculated. Before the MFM experiments were performed, the magnetic stripes were oriented along the preferred direction by applying an in-plane external magnetic field greater than $H_{||}^{\rm sat}$. The width w of the stripe domains can be controlled by the Py thickness d_m following the phenomenological relation $w = \alpha\sqrt{d_m}$ [32]. By a statistical profile-line measurement of w we infer $\alpha \approx 2\sqrt{\mu\text{m}}$. The values of d_m,w,d_s, $M_{\rm cs}$(6 K), and M_{cl}(6 K) are presented in Table I.

III. EXPERIMENTS

We analyzed several Nb/Py heterostructures, fulfilling the conditions $\frac{w}{\lambda} > 1$ and $\frac{d_s}{\lambda} > 1$, so that the formation of spontaneous V-AV pairs only depends upon the magnitude of M_0 at the interface with respect to the critical magnetization $M_{c(s,l)}$. In principle, one can assume that the intensity of M_0 increases with the increase in Py thickness. For this reason, we began by analyzing the behavior of the Nb (200 nm)/Py (4 μm) sample, which should be in a suitable thickness regime to accommodate V-AV.

TABLE I. (Color online) The characteristic parameters of the Py/Nb bilayers and the respective critical magnetization values are shown. By increasing the Py thickness the stripe width also increases following the square root dependence. Note that $M_{\rm cs}$ is always lower than M_{cl} except for the Nb (360 nm)/Py (1 μm) sample.

d_m (μm)	w (nm) + Δw	d_s (nm)	$M_{\rm cs}$ (G)	M_{cl} (G)
4.0	1000 ± 6%	200	16.6	23.3
2.0	790 ± 4%	200	21.1	26.1
		120	11.9	25.2
1.0	490 ± 2%	360	61.5	34.3
		200	33.9	34.2
		150	24.9	33.9
		100	15.1	32.6

Figure 2 presents the MFM maps of Nb (200 nm)/Py (4 μm) samples above and below the superconducting critical temperature, at $T = 12$ K [Fig. 2(a)] and $T = 6$ K [Fig. 2(b)], respectively. This Py thickness is close to a supercritical thickness value, for which vertical alignment starts to fail [33] and, above T_S, we note a soft zig-zag deformation of the expected stripe magnetic template. From a statistical line profile analysis, performed in different areas of the sample surface, we obtained an average stripe width of w = 1000 ± 60 nm, so that $w/\lambda \approx 15$ and $d_s/\lambda \approx 3$. Below T_S, the diamagnetism of the Nb causes a further attenuation of the stripe contrast and spontaneous V-AV are observed at the center of the stripes, concordant with the M_0 down/up magnetization [12]. The V-AV formation indicates that in this sample the threshold condition $M_0 > M_{\rm cs}$ is satisfied, inferring $|M_0| > 17$ G for the out-of-plane component at the Nb/Py interface, a value very much lower than the $H_{c1} = 418$ G needed to nucleate vortices in a single Nb layer. The threshold condition also indicates that V-AV pairs will be formed for any Nb layer thinner than 200 nm.

Figures 3(a) and 3(b) show MFM maps for Nb (200 nm)/Py (2 μm) above and below T_S. For this sample, $w = 790 \pm 35$ nm, $w/\lambda \approx 12$, and $d_s/\lambda \approx 3$. At $T = 6$ K, the formation of spontaneous V-AV pairs with a high and almost uniform density along the stripes is evident. Again, the threshold

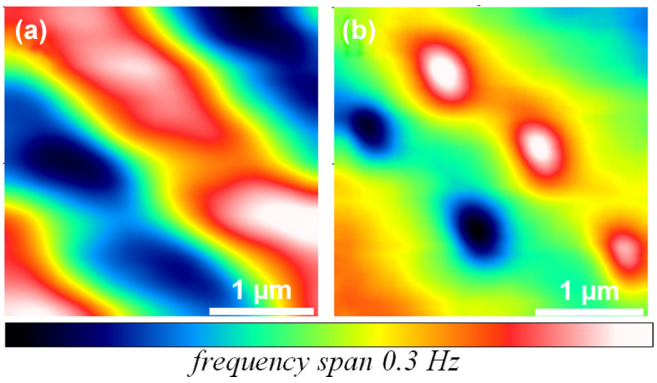

FIG. 2. (Color online) MFM maps of Nb (200 nm)/Py (4 μm), 2.9 μm × 2.9 μm scan area at $h = 60$ nm. (a) $T = 12$ K. (b) $T = 6$ K. Above T_s the characteristic Py magnetic template is shown; below T_s spontaneous V-AV appear concordant with the magnetization polarity.

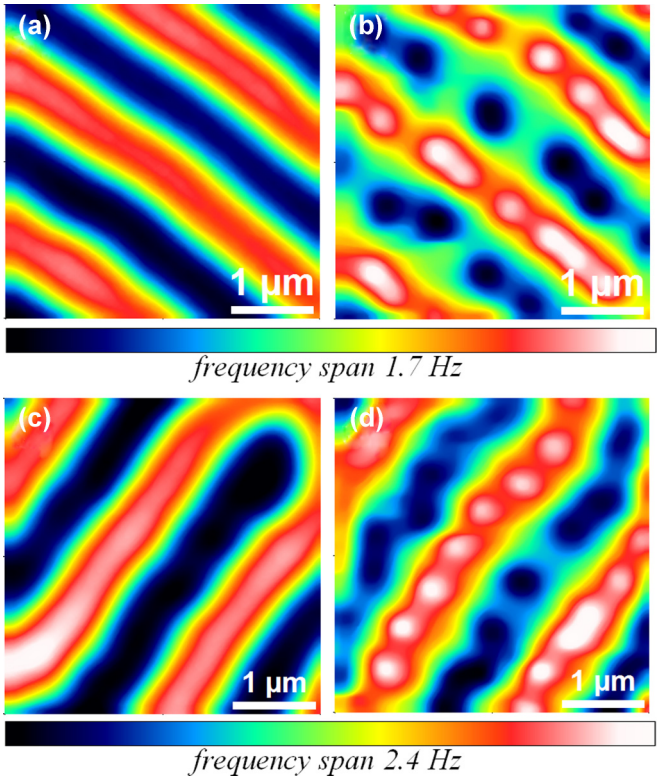

FIG. 3. (Color online) MFM maps of Nb (200 nm)/Py (2 μm), 3.8 μm × 3.8 μm scan area at $h = 180$ nm. (a) $T = 12$ K. (b) $T = 6$ K. MFM maps of Nb (120 nm)/Py (2 μm), 3.8 μm × 3.8 μm scan area at $h = 180$ nm. (c) $T = 12$ K. (d) $T = 6$ K. Below T_S, both Nb (200 nm)/Py (2 μm) and Nb (120 nm)/Py (2 μm) samples show spontaneous V-AV. Note that the MFM maps [panels (c) and (d)] are affected by a small thermal drift.

condition $M_0 > M_{cs}$ is satisfied with $|M_0| > 21$ G at the interface. Indeed, we can verify that, in the case of thinner Nb layers, spontaneous pairs are also formed, as observed in Figs. 3(c) and 3(d) referring to a Nb (120 nm)/Py (2 μm) bilayer with $d_s/\lambda \approx 1.8$. By comparing the frequency spans of the images, we consistently found a major attenuation in Nb (200 nm)/Py (2 μm), as it had the thickest Nb layer. So far we have been getting the indication that spontaneous V-AV pairs can be formed in Nb/Py bilayers, suggesting the possibility to quantitatively evaluate a lower bound for the effective value of M_0.

To systematically evaluate M_0, a more complete set of bilayers Nb (360, 200, 150, and 100 nm)/Py (1 μm) was fabricated with $w/\lambda \approx 7$ and $d_s/\lambda \approx 5 \div 1.5$. However, among these sets of heterostructures, any attempts to unveil spontaneous V-AV in Nb (360, 200, and 150 nm)/Py (1 μm) samples failed (Fig. 4), whereas stable vortex configurations can be formed crossing T_S with an external magnetic field applied, favoring the V or AV nucleation on the top of the corresponding stripes [15]. Figure 5 shows the distribution along the underlying magnetic domains of V in Nb (360 nm)/Py (1 μm) [Fig. 5(a)] and Nb (200 nm)/Py (1 μm) [Fig. 5(b)] and AV in Nb (150 nm)/Py (1 μm) [Fig. 5(c)], nucleated, respectively, by $H = -12$ G, $H = -60$ G, and $H = +12$ G. A more detailed analysis for these samples has been already discussed by the authors [12,14,15].

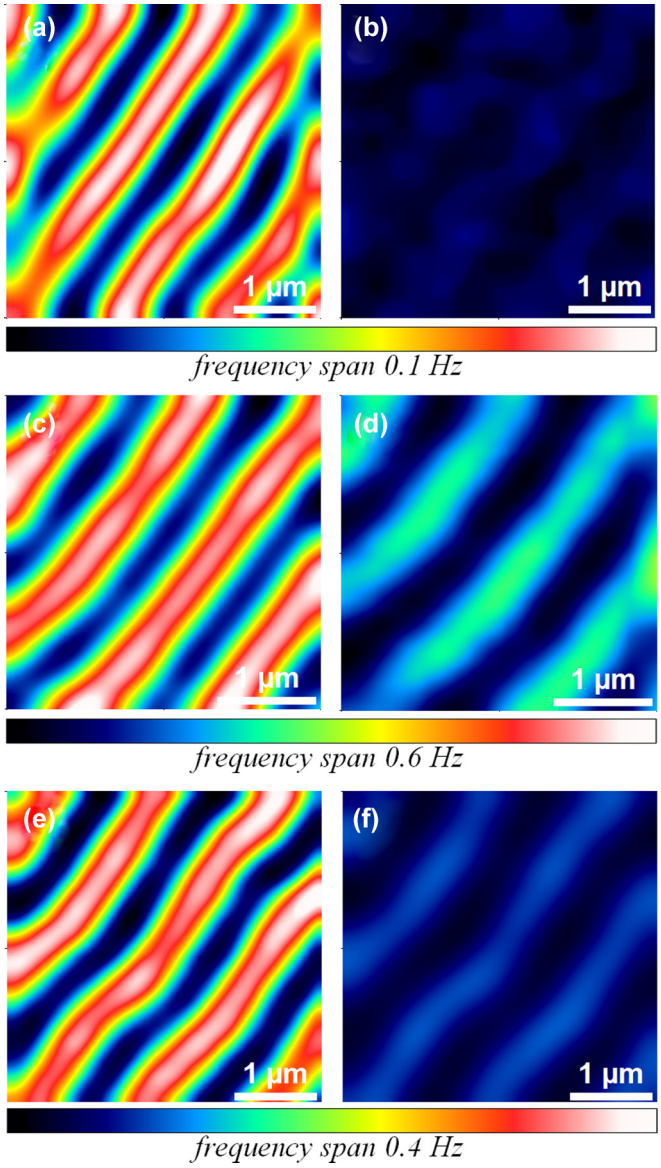

FIG. 4. (Color online) MFM maps of 3.8 μm × 3.8 μm scan areas on Nb (360 nm)/Py (1 μm) at $h = 50$ nm and (a) $T = 12$ K and (b) $T = 6$ K; Nb (200 nm)/Py (1 μm) at $h = 60$ nm and (c) $T = 12$ K and (d) $T = 6$ K; and Nb (150 nm)/Py (1 μm) at $h = 110$ nm and (e) $T = 12$ K and (f) $T = 6$ K. Below T_S, the magnetic contrast of MFM maps is strongly attenuated due to the diamagnetism of the Nb superconducting layer; no occurrences of spontaneous V-AV are measured.

Here we focus our attention on the behavior of the Nb (150 and 100 nm) hybrids shown in Figs. 4(e), 4(f), and 6. The Nb (150 nm)/Py (1 μm) sample was measured at $h = 100$ nm, with a frequency span of 0.4 Hz and $w = 491 \pm 10$ nm. For this sample, any attempt to unveil spontaneous V-AV among a great number of different analyzed areas failed. By contrast, an intensive analysis in different areas of the 100-nm Nb bilayer showed that V-AV pairs were formed.

In Fig. 6, the MFM maps of Nb (100 nm)/Py (1 μm) acquired at $h = 130$ nm, above [Fig. 6(a)] and below [Fig. 6(b)] T_s, are shown. Below T_S, a low density of spontaneous V-AV was verified in different analyzed areas [Figs. 6(b)–6(d)].

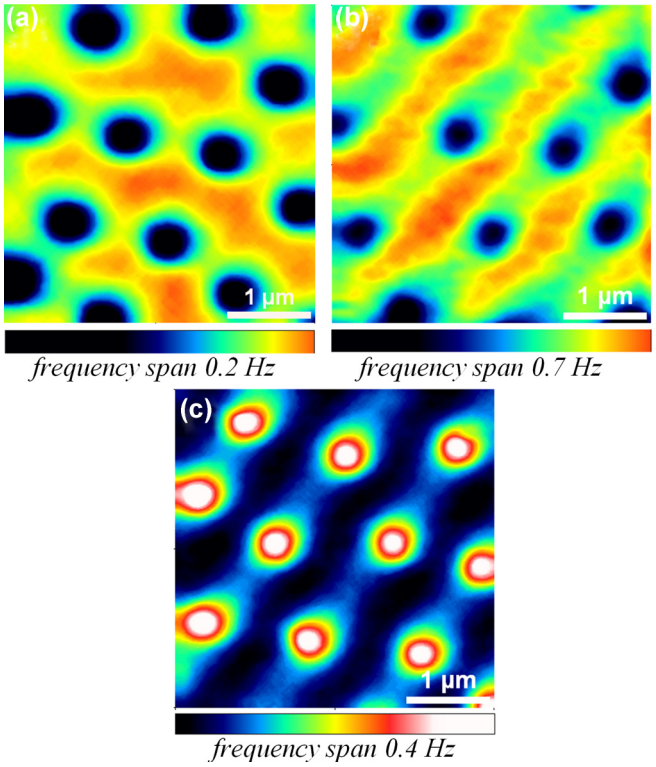

FIG. 5. (Color online) MFM maps of 3.8 μm × 3.8 μm scan areas at $T = 6$ K on (a) Nb (360 nm)/Py (1 μm) at $h = 110$ nm and $H = -12$ G, (b) Nb (200 nm)/Py (1 μm) at $h = 60$ nm and $H = -60$ G, and (c) Nb (150 nm)/Py (1 μm) at $h = 110$ nm and $H = +12$ G. In the absence of spontaneous quantum fluxes, V or AV are nucleated through a field cooling procedure.

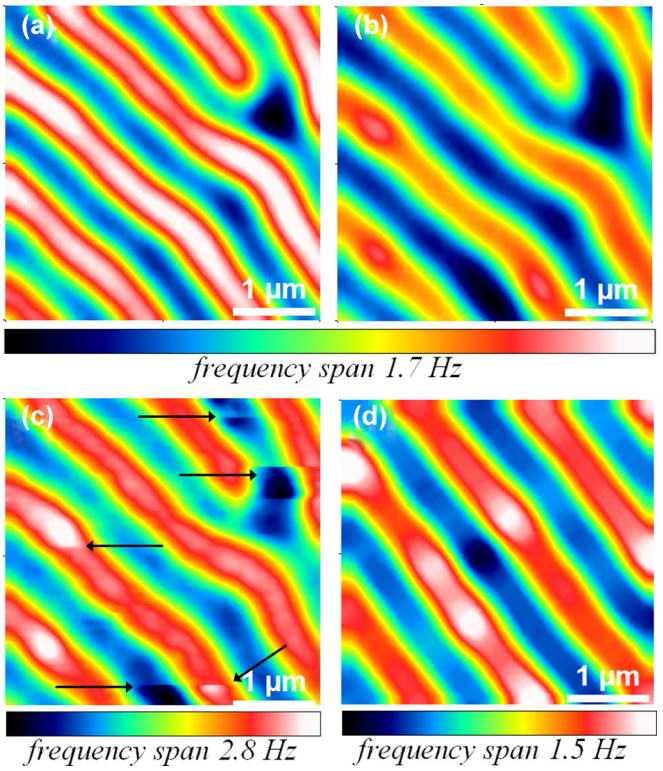

FIG. 6. (Color online) MFM maps of Nb (100 nm)/Py (1 μm), 3.8 μm × 3.8 μm scan area at $h = 130$ nm and (a) $T = 12$ K and (b) $T = 6$ K; (c) at $h = 30$ nm and $T = 6$ K, tip-vortex interaction favors spontaneous V-AV visualization. (d) Different 3.8 μm × 3.8 μm scan area at $h = 100$ nm and $T = 6$ K. Below T_s, the presence of spontaneous V-AV was verified in different analyzed areas.

To maximize the magnetic signal, the tip-sample distance was reduced to $h = 30$ nm [Fig. 6(c)]. By doing this, the frequency span increased from 1.7 to 2.8 Hz and V-AV motion was induced by the stronger tip-vortex interaction. Such V-AV movements appear as instabilities or jumps in the MFM image and are marked with arrows. We emphasize that for images acquired above T_s there are no indications of jumps in frequency at any tip-sample distance. This suggests that these jumps are due to vortex-tip interactions, rather than to domain-tip interactions. For this set of samples, the threshold condition $M_0 > M_{cs}$ is satisfied by 100-nm Nb and is not satisfied by 150-nm Nb. This time we obtain for the 1-μm Py out-of-plane magnetization component an interval of 15.1 G $< |M_0| <$ 24.9 G, still much lower than the superconducting lower critical field for a single Nb layer.

We conclude that the estimate of M_0 is consistent with the measurement of 16 G reported in [12,34], very close to $M_{cs} = 15.1$ G, and should justify the opposite results obtained in an MFM experiment on a similar Nb (100 nm)/Py (1 μm) sample [12], in which no spontaneous V-AV formation was found. Very small fluctuations either in Py stripe width or in magnetization can hinder spontaneous V-AV formation in the 100-nm Nb top layer.

We speculate that for this sample, with lower V-AV density, both the intrinsic Nb pinning and the Py magnetic defects, such as the bifurcation at the top right corner of the Figs. 6(a) and 6(b), play a role in the V-AV spatial distribution.

IV. DISCUSSION

In magnetically coupled Nb/Py heterostructures, the Curie temperature $T_C = 750$ K is much higher than the superconducting critical temperature $T_S = 8.9$ K, ensuring that the superconducting transition always occurs in the nonuniform Py magnetic stray field. This causes the Nb layers to be field cooled and spontaneous V-AV to be formed in the absence of an external magnetic field. In particular, two types of quantum flux penetration can occur: straight vortices, which pierce the superconductor in the middle of the magnetic stripes, and semiloops, which remain within S, with their saddle points at the domain walls.

Just below T_S, the superconducting lower critical field is almost zero, whereas the critical magnetizations for the nucleation of spontaneous vortices $M_{cs} = 0.2\frac{d_s}{w}H_{c1}$ and $M_{cl} = \frac{H_{c1}}{8\ln(4w/\pi\lambda)}$ are obviously lower than M_0. As a consequence, at $T = T_S$, the threshold condition $M_0 > M_{c(s,l)}$ is always satisfied and semiloops or straight vortices are formed in the Nb layers. By decreasing the temperature below T_S, $H_{c1}(T)$ grows from $H_{c1}(T_S) = 0$ G to $H_{c1}(0\text{ K}) = 720$ G, with a corresponding increase in $M_{c(s,l)}$. For this reason, at $T < T_S$, $M_0 < M_{c(s,l)}$ can occur and, in this case, vortices formed at $T = T_S$ can move out from the superconducting layer. In particular, vortices escape from the S layer when $M_0 < M_{c(s,l)}$ and $U_{SV} \ll U_{BL}$, k_BT; i.e., the energy required to pin a vortex $U_{SV} = \frac{1}{4\pi}H_{c1}\Phi_0 d_s$ is much lower than the Bean-Livingston

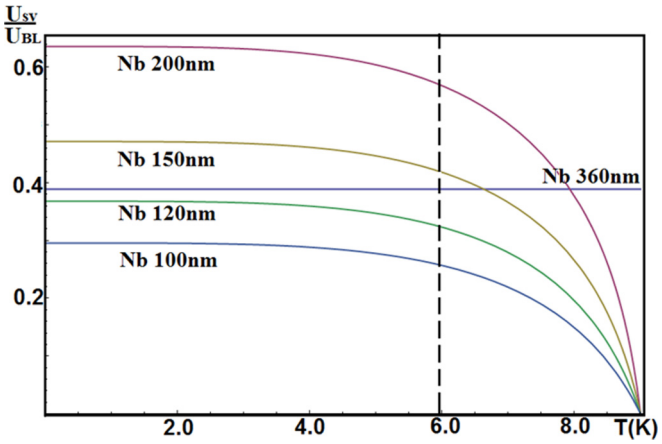

FIG. 7. (Color online) Temperature-dependence of the ratio U_{SV}/U_{BL} of the Nb/Py heterostructures. For the 360-nm Nb case the violet line represents the energy needed to form a semiloop, a quantity that is independent of the temperature.

barrier $U_{BL} = \frac{(\pi+2)}{4\pi} H_{c1} \Phi_0 \lambda$ [35] and the thermal energy. This "escape condition," $U_{SV} \ll U_{BL}$, is always verified for the semiloops, while it is satisfied by the straight vortices only when $d_s \ll (\pi + 2)\lambda$ [18].

With respect to our Nb/Py heterostructures, at a measurement temperature of $T = 6$ K, the values of M_{cs} and M_{cl}, reported in Table I, show an energetically favored formation of straight vortices in all samples, with the exception of Nb (360 nm)/Py (1 μm), in which semiloops are still expected. Note that the MFM technique can only visualize straight V-AV but not semiloops. The temperature-dependence of the U_{SV}/U_{BL} ratio of our Nb/Py heterstructures shown in Fig. 7 is always lower than 1, which indicates that the vortices [semiloops in Nb (360 nm)/Py (1 μm) and straight in the other samples] have to leave the S layer if $M_0 < M_{c(s,l)}$.

As a consequence, considering that we observed no occurrences of V-AV pairs at $T = 6$ K in Nb (150, 200, and 360 nm)/Py (1 μm), M_0 has to be less than $M_{c(s,l)}$ and we can deduce that $M_{0-1\mu m} < 24.9$ G.

By contrast, the MFM observation of straight vortices in Nb (200 nm)/Py (4 μm) and Nb (200 and 120 nm)/Py (2 μm) at $T = 6$ K allows us to infer that $M_{0-4\mu m} > 17$ G and $M_{0-2\mu m} > 21$ G. Similarly, the presence of straight vortices in Nb (100 nm)/Py (1 μm) and their absence in Nb (150 nm)/Py (1 μm) lead us to conclude that 15.1 G $< M_{0-1\mu m} < 24.9$ G. Finally, the inferred value for $M_{0-1\mu m}$ results in lower than the semiloop critical magnetization $M_{cl} = 34$ G, estimated for the Nb (360 nm)/Py (1 μm) sample, indicating that this sample at $T = 6$ K does not form semiloops.

In conclusion, in this paper we present the recent results of cryogenic MFM experiments on S/F hybrids based on Nb/Py heterostructures, fabricated by the sputtering deposition technique. The main goal of our work was to check the presence or the absence at $T = 6$ K of spontaneous V-AV among samples with different thicknesses of both the S and the F layers. We remark that the mechanisms of formation, pinning and depinning of spontaneous semiloops or straight vortices, are nontrivial. Moreover, these phenomena are governed by validity and threshold conditions that take into account the London penetration length, the S and F thicknesses, and the out-of-plane magnetization component of the F layer, as well as by an escape condition based on the U_{SV}/U_{BL} energy ratio. These experiments support the picture described in phenomenological models by Lahio *et al.* [18] and, albeit indirectly, provide a relatively effective method for measuring the canted magnetization in Py thin films via MFM measurements.

ACKNOWLEDGMENTS

Work done at Temple University was supported by the U.S. Department of Energy (DOE), Office of Science, Basic Energy Sciences (BES), Division of Materials Sciences and Engineering, under Grant No. DE-SC0004556. Work at Argonne National Laboratory was supported by the U.S. Department of Energy (DOE), Office of Science, Basic Energy Sciences (BES), under Grant No. DE-AC02-06CH11357. We also acknowledge the support of the MIUR (Italian Ministry for Higher Education and Research) under the project "Rientro dei Cervelli."

[1] M. Baert, V. V. Metlushko, R. Jonckheere, V. V. Moschalkov, and Y. Bruynseraede, Phys. Rev. Lett. **74**, 3269 (1995).

[2] Y. Otani, B. Pannetier, J. P. Nozieres, and D. Givord, J. Magn. Magn. Mater. **126**, 622 (1993); J. I. Martin, M. Velez, J. Nogues, and I. K. Schuller, Phys. Rev. Lett. **79**, 1929 (1997).

[3] J. I. Martin, M. Velez, A. Hoffman, I. K. Schuller, and J. L. Vicent, Phys. Rev. Lett. **83**, 1022 (1999).

[4] J. I. Martin, Y. Jaccard, A. Hoffman, J. Nogues, J. M. George, J. L. Vicent, and I. K. Schuller, J. Appl. Phys. **84**, 411 (1998).

[5] J. I. Martin, M. Velez, J. Nogues, A. Hoffman, Y. Jaccard, and I. K. Schuller, J. Magn. Magn. Mater. **177**, 915 (1988).

[6] A. Angrisani Armenio, C. Bell, J. Aarts, and C. Attanasio, Phys. Rev. B **76**, 054502 (2007).

[7] L. N. Bulaevskii, E. M. Chudnovsky, and M. P. Maley, App. Phys. Lett. **76**, 2594 (2000); Yu. I. Bespyatykh and W. Wasilevski, Phys. Solid State **43**, 224 (2001).

[8] A. A. Garcia-Santiago, F. Sanchez, M. Varela, and J. Tejada, Appl. Phys. Lett. **77**, 2900 (2000).

[9] V. Vlasko-Vlasov, U. Welp, G. Karapetrov, V. Novosad, D. Rosenmann, M. Iavarone, and W. K. Kwok, Phys. Rev. B **77**, 134518 (2008).

[10] G. Karapetrov, J. Fedor, M. Iavarone, D. Rosenmann, and W. K. Kwok, Phys. Rev. Lett. **95**, 167002 (2005).

[11] G. Karapetrov, M. V. Milošević, M. Iavarone, J. Fedor, A. Belkin, V. Novosad, and F. M. Peeters, Phys. Rev. B **80**, 180506(R) (2009).

[12] M. Iavarone, A. Scarfato, F. Bobba, M. Longobardi, G. Karapetrov, V. Novosad, V. Yefremenko, F. Giubileo, and A. M. Cucolo, Phys. Rev B **84**, 024506 (2011).

[13] N. Amos, R. Fernandez, R. Ikkawi, B. Lee, A. Lavrenov, A. Krichevsky, D. Litvinov, and S. Khizroev, J. Appl. Phys. **103**, 07E732 (2008).

[14] M. Iavarone, A. Scarfato, F. Bobba, M. Longobardi, S. A. Moore, G. Karapetrov, V. Yefremenko, V. Novosad, and A. M. Cucolo, IEEE Trans. Magn. **48**, 3275 (2012).
[15] A. M. Cucolo, A. Scarfato, M. Iavarone, M. Longobardi, F. Bobba, G. Karapetrov, V. Novosad, and V. Yefremenko, J. Supercond. Nov. Magn. **25**, 2167 (2012).
[16] G. Carapella, P. Sabatino, and G. Costabile, Phys. Rev. B **81**, 054503 (2010).
[17] G. M. Genkin, V. V. Skuzovatkin, and I. D. Tokman, J. Magn. Magn. Mater. **130**, 51 (1994).
[18] R. Laiho, E. Lähderanta, E. B. Sonin, and K. B. Traito, Phys. Rev. B **67**, 144522 (2003).
[19] G. Maskimova, R. M. Ainbinder, and D. Yu. Vodolazov, Phys. Rev. B **78**, 224505 (2008).
[20] H. Stillrich, C. Menk, R. Frömter, and H. P. Oepen, J. Appl. Phys. **105**, 07C308 (2009).
[21] P. Vavassori, Appl. Phys. Lett. **77**, 1605 (2000).
[22] G. Gubbiotti, G. Carlotti, M. G. Pini, P. Politi, A. Rettori, P. Vavassori, M. Ciria, and R. C. O'Handley, Phys. Rev. B **65**, 214420 (2002).
[23] W. Sucksmith and J. E. Thompson, Proc. R. Soc. London, Ser. A **225**, 362 (1954).
[24] J. J. Krebs, B. T. Jonker, and G. A. Prinz, J. Appl. Phys. **61**, 3744 (1987).
[25] A. Berger and M. R. Pufall, Appl. Phys. Lett. **71**, 965 (1997).
[26] A. Berger and M. R. Pufall, J. Appl. Phys. **85**, 4583 (1999).
[27] L. Louail, K. Ounadjela, and R. Stamps, J. Magn. Magn. Mater. **167**, L189 (1997).
[28] W.-S. Kim, W. Andrä, and W. Kleeman, Phys. Rev. B **58**, 6346 (1998).
[29] K. Ha and R. C. O'Handley, J. Appl. Phys. **87**, 5944 (2000).
[30] L. P. Gor'kov, Zh. Eksp. Teor. Fiz. **36**, 1918 (1959) [Sov. Phys. JETP **9**, 1364 (1959)]; P. H. Kes and C. C. Tsuei, Phys. Rev. B **28**, 5126 (1983).
[31] Y. Murayama, J. Phys. Soc. Jpn. **21**, 2253 (1966).
[32] S. Chikazumi, *Physics of Ferromagnetism* (Oxford University Press, New York, 1997).
[33] L. S. Palatnik, L. I. Lukashenko, Yu. V. Zolotniskiĭ, and B. A. Avramenko, Zh. Eksp. Teor. Fiz. **59**, 1177 (1970) [Sov. Phys. JETP **32**, 643 (1971)].
[34] A. Belkin, V. Novosad, M. Iavarone, J. Fedor, J. E. Pearson, A. Petrean-Troncalli, and G. Karapetrov, Appl. Phys. Lett. **93**, 072510 (2008); A. Belkin, V. Novosad, M. Iavarone, R. Divan, J. Hiller, T. Proslier, J. E. Pearson, and G. Karapetrov, *ibid.* **96**, 092513 (2010).
[35] B. V. Petukhov and V. R. Chechetkin, Zh. Eksp. Teor. Fiz. **65**, 1653 (1973) [Sov. Phys. JETP **38**, 827 (1974)].
[36] J. Ben Youssef, N. Vukadinovic, D. Billet, and M. Labrune, Phys. Rev. B **69**, 174402 (2004).